Laser Spectroscopy of Hydrogen-Like and Helium-Like Ions

Edmund G. Myers

Florida State University, Department of Physics, Tallahassee, FL 32306-4350, USA

Abstract. Laser spectroscopy of hydrogen-like and helium-like ions is reviewed. Emphasis is on the fast-beam laser resonance technique, measurements in moderate-Z ions which provide tests of relativistic and quantum-electrodynamic atomic theory, and future experimental directions.

1 Introduction

Precision measurement of energy intervals in hydrogen and helium has been fundamental to the development of atomic theory. Relativistic and quantum-electrodynamic contributions scale with various powers of Z. Hence more information is gained by extending precise measurements to one- and two-electron ions. Laser spectroscopy is restricted to certain special transitions which fall in the infrared, visible or near-ultraviolet, and from which a useful signal can be obtained. However, where applicable, it provides precision tests of theory. The focus of this review is laser spectroscopy of the $n = 2$ levels of moderate-Z helium-like and hydrogen-like ions. Previous reviews may be found in [1,2,3].

2 Fast-Beam Laser Resonance Technique

The first application of laser spectroscopy to a one-electron ion was a measurement of the $2S_{1/2} - 2P_{3/2}$ interval in F^{8+} by a Rutgers-Bell Labs collaboration [4]. This experiment is the prototype of much subsequent work. The basic technique is illustrated in fig. 1a,b. $^{19}F^{8+}$ ions, of which about 1% were in the metastable $2S_{1/2}$ level, mean lifetime $0.23\,\mu$s, were produced by foil stripping a 64 MeV ($\beta = v/c \simeq 0.075$) beam of lower-charged fluorine ions to F^{9+} from a tandem Van de Graaff accelerator, followed by single-electron capture in a second $5\,\mu\mathrm{gcm}^{-2}$ foil. After a distance of 1 m, corresponding to a time interval of about 50 ns, the ions intersected the beam from a pulsed HBr chemical laser, which induced transitions to the $2P_{3/2}$ level. This level decayed rapidly emitting a 826 eV X-ray which was detected in a proportional counter. Because of the large beam velocity, the laser frequency as seen by the moving ion, ω', is Doppler shifted from the frequency in the laboratory frame, ω_l, according to the relativistic Doppler formula

$$\omega' = \omega_l \gamma (1 - \beta \cos\theta) \tag{1}$$

where $\gamma = (1-\beta^2)^{-1/2}$, and θ is the angle of intersection between the ion and the laser beam in the laboratory frame. The high-power HBr laser output consisted of various fixed frequency lines around 2300 cm^{-1}. The effective laser frequency was scanned across the broad $2S_{1/2}-2P_{3/2}$ resonance by varying the intersection angle.

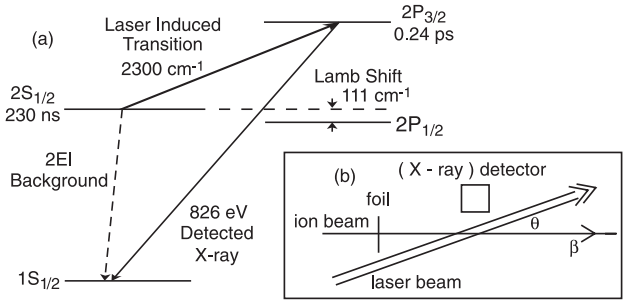

Fig. 1. (a) Energy levels of F^{8+} relevant to the measurement of the $n = 2$ Lamb shift **(b)** Schematic illustrating the fast-beam laser resonance technique

Using a related arrangement, a measurement of the $1s2p\ ^3P_2-^3P_1$ fine structure interval in the two-electron ion F^{7+} was carried out at Oxford [2,5]. Here a continuous-wave CO_2 laser induced the magnetic-dipole transition from $2\,^3P_2$, mean lifetime 10.4 ns, to $2\,^3P_1$, mean lifetime 0.54 ns. The excited F^{7+} ions were produced by stripping 11–17 MeV $F^{3+,4+}$ beams. The fixed frequency laser beam intersected the ion beam at 5° and was tuned across the relatively narrow resonance by varying the beam velocity. The resonance was detected via the X-ray decay of $2\,^3P_1$ to the ground state.

2.1 Signal Formation

Production of highly-charged ions by passing an accelerated lower-charged ion beam through a thin foil is a standard technique of accelerator physics. The cross-section for removing or exciting an electron in the n-shell of the moving ion of nuclear charge Z becomes large when the ion velocity becomes comparable to the Bohr velocity $Z\alpha c/n$. Tables of resulting charge-state distributions can be found in [6]. From the point of view of the moving ion, the foil produces a space-charge compensated electron current pulse of $\sim 10^{14}$ A cm^{-2}, 10 orders-of-magnitude higher in intensity than the electron current density in an electron beam ion trap (EBIT) [7], for example. The high collision frequency is very effective in producing highly-charged ions in excited states. A foil-stripped ion beam from a tandem accelerator could contain 10 particle-nA (nA/charge) in the hydrogen-like charge state, in a beam focused to a diameter of ∼1 mm, with a few mrad divergence. If 1% are in the $2S_{1/2}$ state, the metastable production rate is $\sim 10^9$ s^{-1}.

With the fast-beam technique the region of excited state production – where there is usually a high X-ray background from short-lived states such as the $nP_{1/2,3/2}$ levels – is spatially separated from the region where the laser-induced signal is detected. It is also advantageous to detect fluorescence from a transition well separated in wavelength from the laser, and preferably much shorter in wavelength, so that good detection efficiency can be obtained with reduced sensitivity to the laser light.

Laser induced transition probabilities are often small. This is because the interaction time of the ions with the laser is short (∼ns), and because the relevant matrix elements are small, or else the levels involved have large natural widths. A useful approximate expression for estimating signal strengths for an electric-dipole (E1) transition from a metastable level $|1\rangle$ to a short lived level $|2\rangle$, followed by a spontaneous decay to a third level $|3\rangle$, when the interaction time is long compared to the lifetime of the second level is [8]:

$$dP/dt' = \frac{I'}{2\epsilon_0 c\hbar^2} \frac{A_{23}|\langle 2|d_e|1\rangle|^2}{(\omega' - \omega_0)^2 + (\Gamma/2)^2} \tag{2}$$

where dP/dt' is the laser induced transition probability per unit time for the process $1 \rightarrow 2 \rightarrow 3$, I' is the light intensity, A_{23} is the spontaneous decay rate of level 2 to level 3, d_e is the electric-dipole operator, ω' is the (Doppler-shifted) laser frequency, ω_0 is the transition center frequency (ω', ω_0 are in angular frequency units), and $\Gamma = \Gamma_1 + \Gamma_2$ is the sum of the total decay rates of levels 1 and 2. In eqn. 2 all quantities refer to the rest frame of the moving ion. I' is related to the intensity I_l of the laser in the laboratory frame by $I' = I_l\gamma^2(1 - \beta\cos\theta)^2$. Because of time dilation, the transition probability per unit time observed in the laboratory frame is $dP/dt = (1/\gamma)dP/dt'$ [9]. When evaluating $|\langle 2|d_e|1\rangle|^2$ an appropriate average has to be taken over the initial and final substates of levels 1 and 2 [10].

2.2 Co-linear Geometry and Kinematic Compression

Advantages of a co-linear interaction geometry are the longer interaction time and reduced sensitivity to the angular dependence of the Doppler-shift (since $\cos\theta \simeq 1 - \theta^2/2$). There is usually also an advantage, compared to a transverse laser-ion interaction geometry, as regards reduced Doppler width. For example, an ion beam from a tandem Van de Graaff accelerator focused to a diameter of 1 mm may have an angular divergence $\Delta\theta \simeq 5$ mrad, leading to a large fractional Doppler width of $\Delta\omega/\omega \simeq \beta\Delta\theta \simeq 2.5 \times 10^{-4}$, if the laser is perpendicular to the ion beam. With an accelerated beam, a given energy spread in the laboratory frame, ΔE_l, corresponds to a decreased longitudinal velocity spread $\Delta\beta = (1/\beta)\Delta E_l/Mc^2$, where βc is the mean velocity and M is the ion mass. This reduction in velocity spread, and hence of "temperature" in the co-moving frame, is called kinematic compression. For a typical foil-stripped tandem beam of charge q, $\Delta E \sim 5q$ keV, $\Delta\beta/\beta \sim 10^{-3}$, and $\Delta\omega/\omega \simeq \Delta\beta \sim 5 \times 10^{-5}$. In heavy-ion storage rings, equipped with electron beam cooling, the longitudinal

velocity spread is determined by the competition between intra-beam scattering (IBS) and the cooling force from the electron beam, and fractional spreads $\Delta\beta/\beta \sim 10^{-4} - 10^{-5}$ are typical [11]. For small numbers of ions trapped in the ring a phase transition has been observed, leading to $\Delta\beta/\beta < 10^{-6}$ [12]. Laser cooling of Li^+ 2^3S_1 metastables using the $2^3S_1 - 2^3P_2$ transition [13,14] has resulted in $\Delta\beta/\beta < 10^{-6}$, and Doppler linewidths $\Delta\omega/\omega \leq 4 \times 10^{-8}$ [15]. Such beams have been used to test the relativistic Doppler formula.

2.3 Determination of the Beam Velocity: Doppler-tuned Spectroscopy with Co- and Counter-Propagating Laser Beams

Co-linear geometry leads to maximal sensitivity to the ion beam velocity. This can be measured by magnetic or electrostatic analysis, time-of-flight, or nuclear resonance techniques [16]. In storage rings it can be obtained from the acceleration voltage of the electron cooler beam or the ion orbital frequency. A fundamental problem is that the average velocity of the metastable ions of interest may not be the same as that of the ion ensemble as a whole. The solution is to induce resonances with laser beams propagating in opposite directions, so the Doppler shifts partially cancel. However, compared to spectroscopy on unaccelerated species, relativistic effects are large. Consider an ion moving with velocity $\beta_1 c$ at (a small) angle θ_1 with respect to the direction of a laser beam of laboratory frequency ω_1. When a transition of frequency ω' in the rest frame of the ion comes to resonance, ω' will be related to ω_1 by

$$\omega' = \omega_1\gamma_1(1 - \beta_1 \cos\theta_1), \tag{3}$$

where $\gamma_1 = (1 - \beta_1^2)^{-1/2}$. Likewise, an ion travelling at velocity $\beta_2 c$ will be resonant with a counter-propagating laser beam of frequency ω_2, if

$$\omega' = \omega_2\gamma_2(1 + \beta_2 \cos\theta_2), \tag{4}$$

where θ_2 is defined relative to the direction opposite to the second laser beam. If either laser is continuously tunable, then Eqs. (3) and (4) can be satisfied with $\beta_1 = \beta_2$, $\theta_1 = \theta_2 = 0$, giving the well-known Doppler-free result

$$\omega' = (\omega_1\omega_2)^{1/2}. \tag{5}$$

If the laser frequencies ω_1, ω_2 are fixed (as for a CO_2 laser for example), the beam velocity must be changed between resonances. However, if ω_1 and ω_2 can be chosen so that resonances occur at similar beam velocities, a considerable reduction in sensitivity to the absolute beam velocity is still obtained. In this case one can write

$$\omega'^2 = \omega_1\omega_2[1 + f\{\Delta p, \bar{p}, \Delta(\theta^2), \bar{\theta^2}\}], \tag{6}$$

where $\Delta p = \gamma_2\beta_2 - \gamma_1\beta_1$, $\bar{p} = (\gamma_1\beta_1 + \gamma_2\beta_2)/2$, $\Delta(\theta^2) = \theta_2^2 - \theta_1^2$, and $\bar{\theta^2} = (\theta_1^2 + \theta_2^2)/2$. (It is convenient to express the beam velocity in terms of $p = \gamma\beta$

because this quantity is proportional to the "magnetic rigidity" of the beam). To a very good approximation, typically 1 part in 10^9 [99], the "correction factor" f is given by

$$f \simeq \Delta p + \frac{\Delta p}{2}[\Delta p - \bar{p}^2 - \bar{\theta^2}] - \frac{\Delta(\theta^2)}{2}\bar{p}(1 + \frac{\bar{p}^2}{4}) + \bar{p}^2\bar{\theta^2}... \tag{7}$$

Hence f is mainly sensitive to the change in $\gamma\beta$, Δp, and to the change in laser-ion intersection angle-squared, $\Delta(\theta^2)$. It is relatively insensitive to the harder to measure absolute rigidity, $\bar{p}$, which may include the energy lost in the foil, and the average intersection angle-squared, $\bar{\theta^2}$.

It is also useful to realize that in eqn. 6, ω'^2 can be replaced by $\omega'_1\omega'_2$, where ω'_1 and ω'_2 are frequencies of two *different* transitions in the moving ion, which are brought to resonance with lasers of frequency ω_1 and ω_2 at a similar beam velocity [100]. The laser frequencies ω_1 and ω_2 could also be from different regions of the spectrum (e.g. microwave, IR, UV). This is necessarily the case for spectroscopy on highly-relativistic beams. But it could also be used, for example, to enable the beam velocity to be calibrated for a fine-structure measurement, making use of a well known gross-structure transition. Analogous (and more obvious) expressions can be written for the ratio ω'_1/ω'_2 for the case of two laser beams both propagating nearly parallel, (or antiparallel) to the ion beam. These expressions are useful for obtaining the frequency difference between nearby transitions, such as hyperfine structure and fine-structure splittings [98].

2.4 Wavefront Curvature Effects

So far it has been assumed that the electromagnetic field of the laser experienced by the moving ion can be treated as a plane wave. Particularly for longer wavelength lasers with tightly focused beams perturbations to the plane-wave Doppler formula must be considered. For a laser in a TEM_{00} mode, propagating along the z-axis, a better approximation is the fundamental Gaussian beam [17], where the electric field is given by

$$E(x, y, z, t) = Re[E_0(x, y, z) \exp i\Phi(x, y, z) \exp i(kz - \omega t)], \tag{8}$$

where $E_0(x, y, z)$ describes the Gaussian variation in amplitude, and $\Phi(x, y, z)$ describes the variation in phase occurring along the axis and due to wavefront curvature. After a relativistic transformation to the rest-frame of the moving ion, the phase factor $\exp i\Phi(x, y, z)$ leads to a shift in the instantaneous frequency of the laser, as experienced by the ion. For an ion travelling parallel to the z-axis, and at a distance r from the axis, this is given (in $\mathrm{rad\,s^{-1}}$) by

$$\delta\omega' = -\gamma\beta c\ \partial\Phi/\partial z = \frac{\gamma\beta c}{z_0}\left[\frac{z_0^2}{z^2 + z_0^2}\right]\left[1 + \frac{r^2}{w_0^2}\frac{(z^2 - z_0^2)}{(z^2 + z_0^2)}\right], \tag{9}$$

where w_0 is the laser spot-size parameter, $z_0 = \pi w_0^2/\lambda$ is the confocal parameter, and z is the perpendicular distance from the waist. The first term is due to the

phase shift along the axis and the second term is from the wavefront curvature of the laser beam. A rigorous treatment of the laser-ion interaction involves solving the time-dependent Schrödinger equation and averaging across the various trajectories of the ions. However in cases of multi-transverse mode laser beams it may only be practical to estimate shifts based on the measured laser beam divergence. For two-photon spectroscopy, using counter-propagating beams in a standing wave, curvature effects cancel up to the time-dilation factor. However in co-linear fast-beam saturation spectroscopy the interactions with the pump and probe beams responsible for the signal may occur at different locations and the analysis is more complicated.

2.5 Alternatives to the Beam-Foil Technique

Excited few-electron ions can be produced by stripping in a gas target, or by electron capture to the next higher charge-state in a gas target. This can be useful for producing metastable beams with reduced beam spread [18,19]. The initial fully-stripped or hydrogen-like ions can be obtained from sources of highly-charged ions such as the electron cyclotron resonance ion source (ECRIS) [20], or the electron beam ion source (or ion trap) (EBIS,EBIT) [21,22]. Experiments, with laser detection, have also been carried out on beams of highly-charged ions passing through optically pumped Rydberg vapor targets [23]. Highly-charged ion sources are designed to increase the time the ions spend interacting with energetic electrons inside the source. Metastables can be extracted directly from such sources, but usually only longer-lived ($\gg$ 100 μs) metastables of easily ionized, lower-Z ions.

One- and two-electron ions in excited states can be produced in storage rings by electron capture from an internal gas target or the electron beam used for cooling. Electron capture (recombination) can also be stimulated, and two-step laser stimulated recombination, where the second step is a bound-bound transition, has been used for spectroscopy of Rydberg transitions, e.g. in Ar^{17+} [24] and C^{4+} [25]. Work aimed at achieving higher precision by using two-photon spectroscopy for the second step is in progress [26].

It has been proposed to apply laser spectroscopy to measure ground state hyperfine structure of high-Z hydrogen-like ions extracted from an EBIT and trapped in a cryogenic Penning trap [27,28]. It should then be possible to detect laser induced transitions between ground state hyperfine levels of a *single* trapped hydrogen-like ion using the "continuous Stern-Gerlach" technique [29]. Laser spectroscopy of the $n = 2$ Lamb shift in hydrogen-like ions inside an EBIT has also been studied [30].

3 Hydrogen-like Ions

3.1 Lamb Shift

The spectrum of hydrogen and one-electron ions provides a direct test of bound-state quantum electrodynamics. Except for finite nuclear-size and mass (recoil)

corrections, QED effects can be isolated as the difference between actual transition energies and results of the Dirac formula. The theory of hydrogen and hydrogenic ions has been extensively reviewed [31,32,33,34,35], where [33,34] and [35] focus on light (low-Z and muonium) and heavy (high-Z) systems respectively. The Lamb shift [36] originally referred to the energy separation between the $2S_{1/2}$ and $2P_{1/2}$ levels in a one-electron system, which are degenerate in the Dirac theory, see fig. 1. This separation is due to QED effects and finite nuclear size effects. However the term is often now used to refer to the QED shift of any atomic energy level, particularly of S-states, where the effect is largest.

QED contributions to the Lamb shift consist of electron self-energy and vacuum polarization terms. In one-electron atoms the former is both the larger and the more difficult to calculate and has been the focus of much recent theoretical work. Up to Feynman diagrams including two-loops the self-energy contribution to a hydrogenic energy level can be written as [32]

$$E_{SE} = (\alpha/\pi)[(Z\alpha)^4/n^3]F_n(Z\alpha)m_ec^2 + (\alpha/\pi)^2[(Z\alpha)^4/n^3]H_n(Z\alpha)m_ec^2 \quad (10)$$

where $F_n(Z\alpha)$ and $H_n(Z\alpha)$ can be expressed as a double power series in $Z\alpha$ and $\ln(Z\alpha)^{-2}$. A decade ago the main aim of Lamb shift measurements in hydrogen-like ions was to investigate higher-order terms in $F(Z\alpha)$. However $F(Z\alpha)$ has now been calculated numerically (to all orders in $Z\alpha$) with good accuracy at both high- and low-Z [37,38], and experimental verification has been provided by X-ray measurements of the $1S_{1/2}$ Lamb Shift in U^{91+} [39,40]. In the meantime focus has shifted to the two-loop contribution. In the $Z\alpha$ expansion of $H(Z\alpha)$, the leading term, and term of relative order $Z\alpha$ have been obtained [41,42]. For terms of relative order $(Z\alpha)^2$, only contributions from some Feynman diagrams (the loop-after-loop correction) have been calculated [43,44,45], including a logarithmic contribution of relative order $(Z\alpha)^2 ln^3(Z\alpha)^{-2}$ [46]. There is disagreement about these calculations and the usefulness of the $Z\alpha$ expansion. Lack of knowledge of these higher-order terms now limits the precision with which recent ultra-precise two-photon spectroscopy of atomic hydrogen [47,48,49] can be used to obtain values for the proton charge radius and the Rydberg constant.

3.2 Experimental Considerations

The $2S_{1/2} - 2P_{1/2}$ (Lamb shift) and $2S_{1/2} - 2P_{3/2}$ (fine structure – Lamb shift) transitions are in principle accessible to laser spectroscopy over a wide region of Z using far-infrared to ultraviolet lasers, spanning the range ∼100–50,000 cm^{-1}. A serious problem is the large natural width of the transition, due to the short lifetime of the $2P$ levels. The radiative decay rate $A(2P-1S) \simeq 6.3\times10^8\, Z^4\, \mathrm{s}^{-1}$ [50]. The Lamb shift increases with Z somewhat more slowly than Z^4, and the ratio of the QED shift to the natural linewidth decreases from 10.6 for hydrogen, to about 4 at $Z = 15$. Precision spectroscopy thus requires the centroid of a resonance to be determined to a small fraction of the linewidth. A frequency scan across the $2S_{1/2} - 2P_{3/2}$ resonance involves a smaller fractional change in the laser wavelength, typically 1–2%, and so is more amenable to laser spectroscopy than the $2S_{1/2} - 2P_{1/2}$ transition.

From eqn. 2, the expected signal for a transition $2S-2P$ followed by spontaneous decay to $1S$ varies as $|\langle 2P|d_e|2S\rangle|^2/A(2P-1S) \sim Z^{-6}$. X-ray backgrounds from the decays of the $2S_{1/2}$ level increase according to $A(2E1) \simeq 8.23\,Z^6\,\mathrm{s}^{-1}$ [51], and as $A(M1) \simeq 2.50\times10^{-6}\,Z^{10}\,\mathrm{s}^{-1}$ [52]. Hence the expected signal-to-background ratio falls as Z^{-12} or faster. It is difficult to see how the technique could be extended to Z above 20. On the other hand, X-ray spectroscopy of $2P-1S$ transitions, which is applicable to all Z, has not yet produced ground state Lamb shift measurements with uncertainties less than 1-2% [39,40,53,54].

3.3 Lamb Shift Measurements in F^{8+}, P^{14+}, S^{15+} and Cl^{16+}

The pioneering laser measurement of Kugel *et al.* [4] on the $2S_{1/2}-2P_{3/2}$ transition in F^{8+} attained a precision equivalent to 1% of the Lamb shift. Comparable precisions were obtained in neighboring ions using the Stark-quenching technique [1]. The same group achieved a precision of 0.7% for the Lamb Shift in a measurement of the $2S_{1/2}-2P_{1/2}$ interval in Cl^{16+} [55], using a line-tunable CO_2 laser and a combination of frequency and angle tuning. The laser system consisted of a scientific CO_2 laser seeding a large (13 m long) amplifier, based on a slow-axial-flow, industrial laser. This was operated in a long-pulsed mode with 120 μs, 175 W pulses, at 480 Hz. All subsequent measurements have been of the $2S_{1/2}-2P_{3/2}$ interval using pulsed dye lasers, which were tuned across the resonance at a fixed beam energy and intersection angle. Using a nitrogen-pumped tunable dye laser (7 ns, ~200 kW pulses at 50 Hz) Pellegrin *et al.* [56] achieved a precision equivalent to 1.2% for the Lamb Shift in P^{14+}. This experiment made use of synchronization of the laser to ion pulses from a cyclotron. The most extensive development has been done by von Brentano and collaborators, who used a specially constructed flash-lamp pumped dye laser (6 μs, ~200 kW pulses at 2 Hz) for measurements on S^{15+} [57] and P^{14+} [58]. They achieved precisions of 0.25% and 0.14% for the Lamb shifts in the two ions respectively. The last four measurements, together with results from the Stark-quenching technique at $Z=16$ and 18, are compared with theory in table 1 (taken from [37]).

It can be seen that the theoretical values are consistently larger than the experimental values, and that the most precise measurements are those using the laser resonance technique. But even here, the most precise experiments, at $Z=15$ and 16, show discrepancies with theory at only the level of one experimental error bar.

3.4 Future Prospects for Laser Lamb Shift Measurements

The largest source of uncertainty in the above experiments was limited statistics. If the centroid of a resonance of FWHM $\Delta\omega$ is to be located to an uncertainty σ_ω, then the number of laser-induced signal counts acquired, S, must satisfy $S^2/(S+B) \gg (\Delta\omega/\sigma_\omega)^2$, where B is the number of background counts acquired in the same time. With the flash-lamp pulsed dye-laser experiments the high pulse power gave good S/B. The poor statistics were due to the low duty cycle

Table 1. Lamb shift in mid-Z hydrogen-like ions

Z	Reference	Experiment [THz]	Theory [THz]
15	Pellegrin *et al.* [56]	20.13(20)	20.23(2)
15	Pross *et al.* [58]	20.188(29)	
16	Zacek *et al.* [59]	25.14(24)	25.34(3)
16	Georgiadis *et al.* [57]	25.266(63)	
17	Wood *et al.* [55]	31.19(22)	31.30(4)
18	Gould and Marrus [60]	37.89(38)	38.19(6)

of the laser $\sim 10^{-5}$, mis-matched to the continuous ion beam from the tandem accelerator. The use of a high power pulsed laser also led to problems of optical damage, and difficulties with measuring the laser frequency, power and overlap with the ion beam, as the laser is tuned across the resonance. Uncertainty in the beam velocity was a significant, but not dominant source of error in [57,58]. This can be reduced by application of counter-propagating beam methods.

The statistics obtained with high-power pulsed lasers would be improved by matching of the ion beam to the laser, by using a pulsed ion source and ion bunching techniques, or a storage ring. A problem is that this leads to very high count rates during the laser pulses which the X-ray detectors must record without saturation. It is worth noting that the Ti:sapphire laser, either flash-lamp pumped, or continuous wave/mode-locked, could be applied to a measurement on hydrogen-like silicon.

Measurement in N^{6+} with a Continuous-Wave CO_2 Laser

Another approach is to work at lower Z so adequate signal-to-background can be achieved using a continuous-wave laser. The $2S_{1/2} - 2P_{3/2}$ transition in N^{6+} is near 12.0 μm and is accessible to the CO_2 laser. An exploratory measurement [61] has been carried out using a 35 MeV N^{6+} beam and the CO_2 laser system described in section 4.3 below, but with a 4° intersection angle. With cw powers of 150 W a signal rate of $10^5\,s^{-1}$/particle-na and S/B of about 20 were obtained. This signal is consistent with the goal of measuring the $2S_{1/2} - 2P_{3/2}$ interval to a few ppm, sufficient to probe the two-loop binding corrections. A more refined measurement using two isotopic CO_2 lasers is in progress [62].

Two-Photon Spectroscopy of the $2S_{1/2} - 3S_{1/2}$ transition in He^+

In high precision two-photon spectroscopy of hydrogen the large natural width of the $2P$ level is avoided by measuring $nS - n'S, D$ transitions [47,48,49]. In He^+

the $2S-3S$ transition occurs with two photons at 338 nm. A measurement using a frequency-doubled dye laser with a resonant build-up cavity is in progress [63]. The $2S-3S$ transition is 100 times narrower than the $2S-2P$ transition. He^+ $2S_{1/2}$ metastables are obtained directly from an electron-bombardment ion source and decelerated to about 2 eV. Detection is via the $3S-2P-1S$ cascade (164 nm and 30 nm) using a silicon photo-diode and a channeltron. The absolute frequency calibration makes use of an iodine stabilized diode laser. Once a signal is obtained, a precision for the He^+ Lamb shift better than 10% of the 16 MHz linewidth is expected. With subsequent improvement the precision should be competitive with the quench-anisotropy measurement of the He^+ $2S_{1/2}-2P_{1/2}$ interval by van Wijngaarden *et al.* [64]. They obtained 14041.13(17) MHz, in good agreement with their theoretical value of 14041.18(13) MHz.

3.5 Ground-state Hyperfine Structure of High-Z Hydrogen-like Ions

For some very highly charged hydrogen-like ions, e.g. $^{209}Bi^{82+}$ and $^{207}Pb^{81+}$, the ground state hyperfine structure splitting is an optical transition. Hence the splitting can be measured by laser excitation of the M1 transition from the lower hyperfine level [65,66]. Measurements were conducted using ~200 MeV/u beams of hydrogen-like ions in the heavy-ion storage ring ESR at GSI. The experiment on ^{209}Bi used an excimer-pumped pulsed dye-laser. The experiment on ^{207}Pb used a pulsed, frequency-doubled, Nd:YAG laser parallel to the ion beam, with Doppler-tuning; and a Nd:YAG pumped optical-parametric oscillator at 1900 nm antiparallel to the ion beam. In each case the delayed, Doppler-shifted fluorescence was detected using photo-multiplier tubes. These measurements are sensitive to higher-order QED corrections, but also to the charge distribution (Breit-Schawlow effect), and especially the magnetization distribution (Bohr-Weisskopf effect), of the respective nuclei.

4 Helium-like Ions

Helium and helium-like ions are the prototypical many-electron system. All the bound-state QED physics of one-electron atoms is still present, of course, but with considerable added complication due to the electron-electron interaction.

By identifying common terms in approaches based on the non-relativistic Schrödinger equation with matrix elements of the Breit-Pauli operators [50,67], and results of a perturbation expansion based on Dirac eigenvalues and matrix elements of the Breit interaction, Drake produced a "Unified" tabulation of ground state and $n=2$ energy levels for all Z [68]. This approach obtained all "structure" contributions of orders $(Z\alpha)^2/Z^p$, $(Z\alpha)^4/Z^p$, $(Z\alpha)^{2n}$ and $(Z\alpha)^{2n}/Z$ (in units of m_ec^2, where $n,p=1,2..$). QED corrections were added making use of results for hydrogen-like ions [31] with an approximate treatment of two-electron corrections of order $\alpha^5Z^3\ln\alpha$ and $\alpha^5Z^3m_ec^2$ [69,70,71]. More recently

the ground state and $n = 2$ energies of all helium-like ions have been calculated relativistically using the Breit equation and a no-pair Hamiltonian formulation [72], by many-body perturbation theory (RMBPT) [73], by configuration interaction theory [74,75], and by "all-orders" many-body theory [76]. These calculations, except at lower Z where they lose accuracy, reproduce the "structure" terms of [68]. In addition, they include a term of order $(Z\alpha)^4\alpha^2 m_e c^2$. But they do not address explicit QED corrections of this order. Multi-configuration Dirac-Fock (MCDF) codes have also been applied to helium-like ions, e.g. see [77].

It *is* possible to formulate multi-electron atomic theory completely as a problem in bound-state QED [35,78]. This approach is most useful at high Z where the electrons can be initially considered hydrogenic, and interactions with the radiation field (including electron-electron photon exchange), are treated as perturbations. This can be shown to reproduce RMBPT ("structure"), along with other explicit QED terms. Calculations have been carried out for the ground state energies of high-Z helium-like ions [79,80] and recently extended to $n = 2$ states [81,82].

Much recent theoretical work has been devoted to atomic helium [83,84,85], and in particular to the $1s2p\,^3P$ fine structure [86,87]. It is aimed to calculate the larger, approx. 30 GHz, $J = 0-1$ interval to better than 1 kHz. With comparably precise experiments this will yield a new value for the fine structure constant. Only J-dependent terms must be considered, and the theory now includes terms up to order α^6 and $\alpha^7 \ln\alpha\ m_e c^2$ [88,89]. Operators for the terms of order α^7 have been evaluated by Zhang [86] and their evaluation is in progress [90]. Contributions of order α^7 have also been obtained using an effective Hamiltonian procedure by Pachucki and Sapirstein [91]. Refs. [88,89] also give results for helium-like ions up to $Z = 12$. Progress has also been made in evaluating the two-electron Bethe-logarithm [92].

4.1 Experimental Considerations

The $n = 2$ levels of helium-like ions, with their principal decay modes [93,94,95], are shown in fig. 2. Here there are two metastable levels, $2\,^3S_1$, with lifetime $\propto Z^{-10}$ due to a relativistic M1 decay, and $2\,^1S_0$, with lifetime $\propto Z^{-6}$ due to a two-photon E1 decay. Important for precision spectroscopy, the $2\,^3P$ levels are much longer lived than the $2\,^1P_1$ level, or the $2P$ levels of hydrogen-like ions of the same Z, since their ground state decays are not fully-allowed E1 transitions. For low-Z the $2\,^3P$ levels decay primarily to $2\,^3S_1$ with rates approx. $\propto Z$. But as Z increases, $2\,^3P_1$ mixes with the $2\,^1P_1$ level due to relativistic interactions, and decays to the ground state with a rate initially increasing approx. as Z^{10}. This becomes the fastest decay mode of this level for $Z > 6$. The $2\,^3P_2$ level can decay to the ground state by a magnetic-quadrupole interaction with rate scaling approx. as Z^8. This mode becomes dominant for $Z > 18$. Finally, $2\,^3P_0$ can mix with $2\,^3P_1$ due to the hyperfine interaction in ions with nuclear spin, and hence also decay to the ground state [96]. The lifetimes of these levels (excluding hyperfine quenching) are shown for different Z in fig. 3.

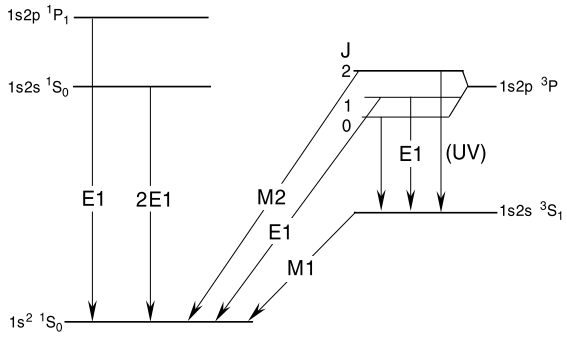

Fig. 2. Schematic of the $n = 2$ levels of helium-like ions showing the principal decay modes

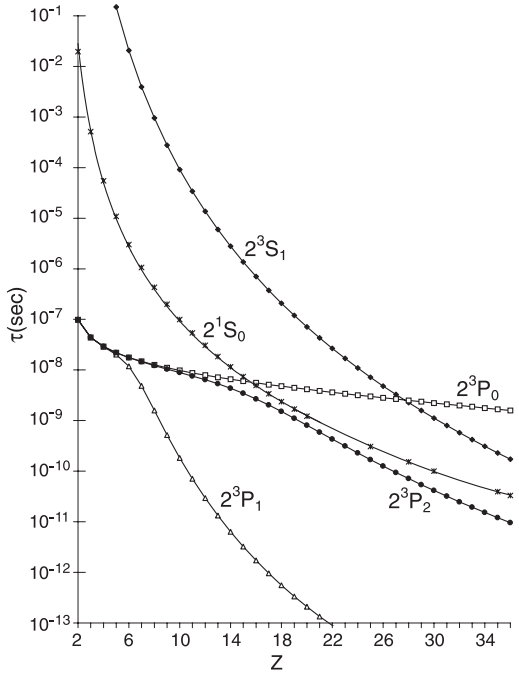

Fig. 3. Mean lifetimes of the $n = 2$ levels of helium-like ions

The energies of the allowed E1 $2\,^3S_1 - 2\,^3P_J$ transitions scale approx. as Z and lie the vacuum ultraviolet ($\lambda < 200\,\mathrm{nm}$) for $Z > 6$. However, the relativistically-allowed $2\,^1S_0 - 2\,^3P_1$ (intercombination) transition lies in the laser-accessible infrared up to $Z \simeq 40$ [97,68], see fig. 4. This transition has the further advantage that the QED contribution is a much larger fraction of the total interval. Due to hyperfine mixing the $2\,^1S_0 - 2\,^3P_0$ transition is also observable in special cases [98].

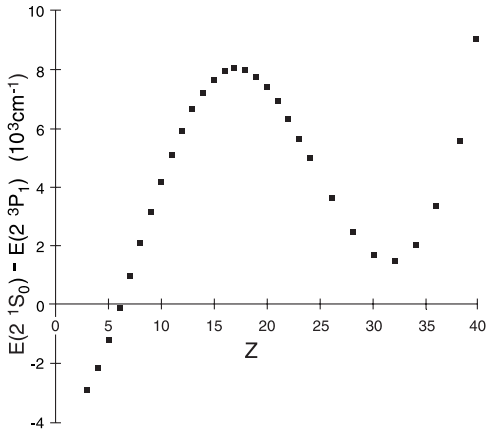

Fig. 4. The intercombination interval $\Delta E(1s2s\ ^1S_0 - 1s2p\ ^3P_1)$ versus Z

It is interesting to consider a figure-of-merit, $\mathcal{Q}_{QED} = \Delta E_{QED}/(\hbar\Gamma)$, where ΔE_{QED} is the total QED contribution to the transition energy and $\hbar\Gamma$ is the total natural width. This is plotted against Z for the four transitions in fig. 5. The potential experimental sensitivity to QED is much higher than for hydrogen-like ions, particularly for the $2\,^3S_1 - 2\,^3P_0$, $^3P_2$ transitions with $Z > 6$. Unfortunately this is also the region where laser spectroscopy with current technology becomes difficult. For the $2\,^3S_1 - 2\,^3P_1$ and $2\,^1S_0 - 2\,^3P_1$ transitions, $\mathcal{Q}_{QED}$ falls off above $Z = 6$ due to the ground state decay of $2\,^3P_1$. Nevertheless, the laser accessible $2\,^1S_0 - 2\,^3P_1$ transition still has a large linewidth advantage over the hydrogen-like $2S - 2P$ transitions at the same Z. The $2\,^1S_0 - 2\,^1P_1$ transition has no linewidth advantage over the hydrogen-like transition.

The matrix elements for the $2\,^3S - 2\,^3P$ transitions are similar to the $2S - 2P$ hydrogenic matrix elements at the same Z. Provided the Doppler width can be reduced so that natural broadening dominates, eqn. 2 shows that the laser induced transition probability for the $2\,^3S - 2\,^3P_0, 2\,^3P_2$ transitions is larger than for the hydrogen-like ion, and falls off more slowly with Z, as Z^{-3}. However there is the problem that the fluorescence must be detected against a background of similar wavelength scattered laser light. For the $2\,^1S_0 - 2\,^3P_1$ transition with $Z > 6$, if the X-ray decay to the ground state is detected, the laser induced signal is comparable to the hydrogen-like case, and falls as Z^{-6}. Here the main

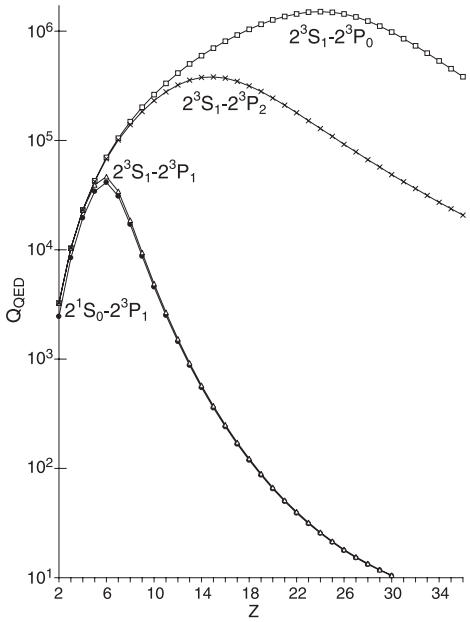

Fig. 5. QED contribution to the energy interval divided by the natural linewidth for the $1s2s\ ^3S_1 - 1s2p\ ^3P_J$ and $1s2s\ ^1S_0 - 1s2p\ ^3P_1$ transitions

backgrounds are from the 2E1 decay of $2\,^1S_0$ and the M1 decay of $2\,^3S_1$, and so scale as Z^6 or Z^{10}. As for laser Lamb shift measurements on hydrogen-like ions, the practical limit for measurements of the $2\,^1S_0 - 2\,^3P_1$ interval is $Z \simeq 20$.

Direct measurements of the $1s2p\ ^3P_0 -^3 P_1$ and $1s2p\ ^3P_2 -^3 P_1$ fine structure intervals use a laser to induce the M1 transitions between them [5,100,101]. The initial level is either $2\,^3P_0$ or $2\,^3P_2$ (mean lifetimes a few ns) and detection is via the X-ray decay of the shorter lived 2^3P_1 to the ground state. Such measurements test higher-order QED corrections to the theory of the fine structure and are relevant to the problem of obtaining α from the fine structure of helium [89]. The $2\,^3P_2 - 2\,^3P_1$ and $2\,^3P_1 - 2\,^3P_0$ intervals are shown in fig. 6. The level ordering is completely inverted for He; the "natural" ordering is achieved by N^{5+}. The $0-1$ interval inverts again for $Z > 45$. In fig. 7 the natural linewidth, as a fraction of the transition interval, is also shown. Particularly for the $2-1$ interval near $Z = 7$ there is a considerable fractional linewidth advantage compared to helium. A fine structure measurement on a moderate-Z helium-like ion could, ultimately, achieve a higher precision than can be obtained in helium. If the theory could be developed to match this precision (which does not appear possible at present), this would lead to a more precise determination of the fine structure constant.

The M1 transition matrix element is $\sim \mu_b$, independent of Z. Hence the laser induced signal for transitions to $2\,^3P_1$ falls as Z^{-10}. The main X-ray background

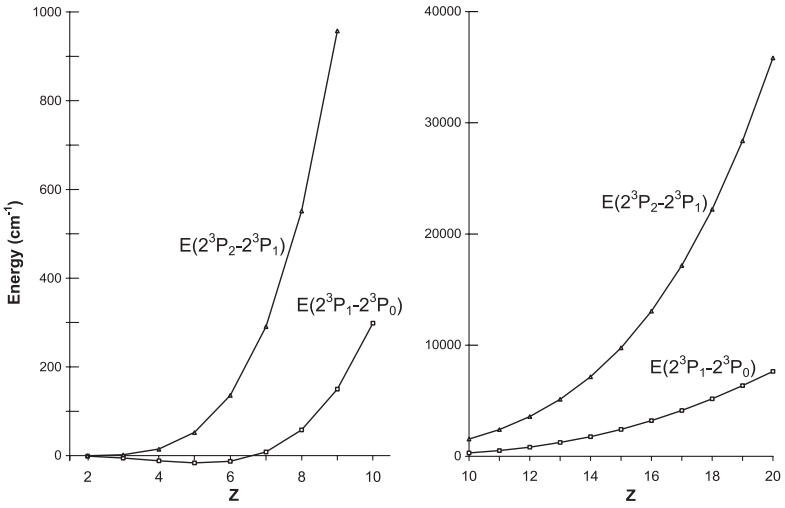

Fig. 6. The fine structure intervals $\Delta E(1s2p\ ^3P_1 - \ ^3P_0)$ and $\Delta E(1s2p\ ^3P_2 - \ ^3P_1)$

is usually from the M2 decay of $2\,^3P_2$. Hence the signal-to-background ratio falls as Z^{-18}. The technique appears to have a practical limit below $Z = 20$.

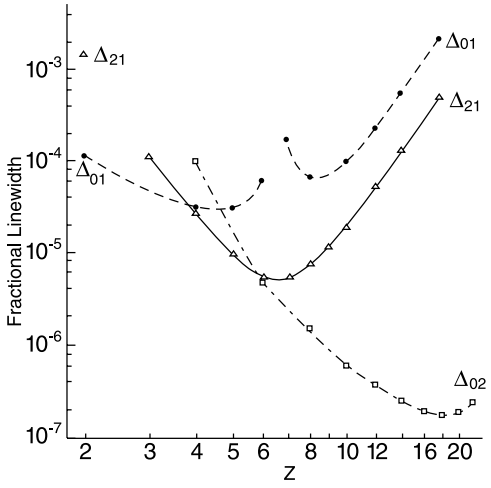

Fig. 7. Natural linewidth divided by the total transition energy for the $1s2p\ ^3P_0 - \ ^3P_1$, $1s2p\ ^3P_2 - \ ^3P_1$ and $1s2p\ ^3P_0 - \ ^3P_2$ fine structure intervals

The $2\,^3P - 2\,^3S$ transitions have been studied extensively using classical UV spectroscopy, e.g. [102,103,104,105]. At the precisions obtainable, the results are generally well described by the "Unified" or relativistic theories, e.g. see [76].

4.2 $2^3S_1 - 2^3P_J$ Transitions in Li^+, Be^{2+} and B^{3+}

Precision measurements of the $2\,^3S_1 - 2\,^3P_J$ transitions in Li^+ [106], Be^{2+} [107] and B^{3+} [108], have been made using co-linear spectroscopy with tunable, cw lasers. Earlier laser work with Li^+ may be found in [109,110,111]. A co-linear measurement of the $2\,^1S_0 - 2\,^1P_1$ interval in Be^{2+} is described in [112]. Ion beams containing $2\,^3S_1$ or $2\,^1S_0$ metastables were extracted from ion sources: a discharge source, an electron-bombardment source, and an ECRIS, for Li, Be and B respectively. All the measurements used counter-propagating laser beams, allowing for the Doppler shift using eqn. 5. For Li^+ [106] two dye lasers were used, and a "Doppler-free" saturated fluorescence signal of 20 MHz FWHM was obtained. The total Doppler width was about 100 MHz at an ion beam energy of 100 keV. For the Be^{2+} $2\,^3S - 2\,^3P$ measurement a frequency-doubled Ti-sapphire laser was used, and for B^{3+}, a frequency-doubled dye laser. With only one laser it was necessary to scan resonances alternately, reversing the direction of the laser between scans, and to rely on the energy stability of the ion beam. For Be^{2+} $2\,^3S - 2\,^3P$ the beam energy was 15 to 20 keV, with a Doppler width of 850 MHz, while for B^{3+} the beam energy was 30 keV and the Doppler width was 1 GHz. In the case of Be^{2+} $2\,^1S_0 - 2\,^1P_1$, the resonance width was approx. 20 GHz, dominated by natural broadening. All experiments made use of "post-acceleration". A voltage was applied to an electrode surrounding the interaction region to fine tune and modulate the beam velocity. The principal background in all three experiments was scattered laser light. The laser frequency calibration used I_2 reference lines.

The largest source of uncertainty quoted in the Li^+ measurement was a systematic error of 250 kHz for possible mis-alignment of the laser and ion beams, the remaining error being due to the calibration (120 kHz) and statistics. For both Be^{2+} experiments the main uncertainty was statistical, from fitting the data and from ion beam energy drift. For B^{3+} the quoted errors are mainly statistical. But, presumably to allow for possible systematic errors, the assigned error was three standard deviations of the mean. All the $2\,^3S - 2\,^3P$ measurements required analysis of the hyperfine structure to extract the "hyperfine-free" transition energies because of mixing of the fine structure due to the hyperfine interaction. Results for the $2\,^3S_1 - 2\,^3P_J$ transitions for each of the three ions are shown in table 2. The result of the Be^{2+} $2\,^1S_0 - 2\,^1P_1$ measurement was 16276.774(9) cm^{-1}. For the $2\,^3S - 2\,^3P$ measurements the errors, as a fraction of the total QED contributions to the intervals, were 11 ppm for Li^+, 70 ppm for Be^{2+}, and 880 ppm for B^{3+}. This precision exceeds that of the theory for higher-order relativistic and QED corrections. The theory for Li^+ in [106] indicates that the expansion in $1/Z$ is too poorly convergent to enable isolation of the order $(Z\alpha)^4\alpha^2 m_e c^2$ term given by the relativistic theories [73,74,75,76], and that the QED uncertainty was at best 30 MHz, or about .1% of the QED correction. Similar analyses for Be^{2+} and B^{3+} are yet to be published. As regards the 2^3P fine structure (see later), the results for Li^+ and B^{3+} are in agreement with the calculations of [88,89]. But for the $J = 2 - 1$ interval in Be^{2+} there is a discrepancy of 6 times the combined experimental and theoretical uncertainty.

Table 2. Experimental $1s2s\ ^3S_1 - 1s2p\ ^3P_J$ intervals in Li^+, Be^{2+} and B^{3+}. Units are MHz for Li^+, and cm^{-1} for Be^{2+} and B^{3+}.

Ion	Reference	$2\,^3S_1 - 2\,^3P_0$	$2\,^3S_1 - 2\,^3P_1$	$2\,^3S_1 - 2\,^3P_2$
$^6Li^+$	Riis [106]	546 525 935.34(36)	546 370 231.34(44)	546 432 908.30(43)
$^7Li^+$	Riis [106]	546 560 683.07(42)	546 404 978.80(51)	546 467 657.21(44)
$^9Be^{2+}$	Scholl [107]	26 864.6120(4)	26 853.0534(3)	26 867.9484(3)
$^{11}B^{3+}$	Dineen [108]	35 393.627(13)	35 377.424(13)	35 430.084(9)

4.3 $2\,^1S_0 - 2\,^3P_1, 2\,^3P_0$ Intercombination Transitions in N^{5+}

The $1s2s\ ^1S_0 - 1s2p\ ^3P_{1,F}$, $^3P_0$ intervals in helium-like nitrogen have been measured by Doppler-tuned co-linear spectroscopy using a CO_2 laser [97,98,99], see fig. 8. A 5-7 MeV N^+ beam obtained from a Van de Graaff accelerator was stripped to N^{5+}, of which about 0.25% was in the $2\,^1S_0$ state, mean lifetime 1.06 μs, by passing it through a 4 $\mu g\,cm^{-2}$ carbon foil. The ions then passed through a 90° analysing magnet, traveling a total distance of 10 m to the interaction region. The 6 m discharge length, grating tuned, slow-axial-flow cw CO_2 laser induced transitions to the $2\,^3P_1$ or $2\,^3P_0$ levels. These were detected via the 190 nm photons emitted in the subsequent $2\,^3P - 2\,^3S$ decays using photomultiplier tubes.

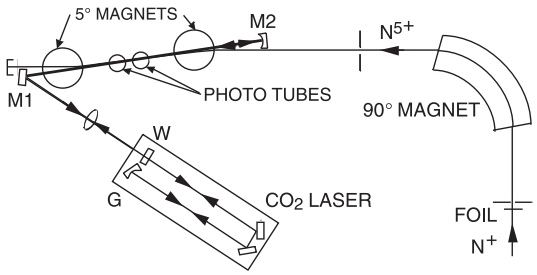

Fig. 8. Schematic of setup used for co-linear laser spectroscopy on N^{5+}

In an initial experiment [97], spectroscopy was performed with the output beam of the unmodified laser counter-propagating to the ion beam. The beam velocity was measured using nuclear resonance and time-of-flight techniques. The weak, hyperfine-induced $2\,^1S_0 - 2\,^3P_0$ resonance was then observed [98], see fig. 9. This enabled the $J = 0 - 1$ fine structure splitting to be obtained by using suitable laser lines to take account of most of the frequency difference, and then measuring the small interval in beam velocity between the resonances.

Subsequently, the setup was modified by extending the laser cavity so that the interaction region occurred at an intracavity waist [99], as in fig. 8. This provided co-and counter-propagating laser beams at the interaction region, but also more laser power, particularly for low-gain laser lines. Powers $> 150\,\mathrm{W}$ cw could be obtained on approx. 100 vibrational-rotational lines across both regular bands, and the "hot" band of $^{12}C^{16}O_2$, spanning a wavelength range of $9.14 - 11.22\,\mu$m. The laser ran multi-longitudinal mode. To sufficient accuracy, the frequency of the laser could be assumed to be that of the laser line centers. These have been measured with metrological precision [113]. Using this system it was possible to measure all three $2\,^1S_0 - 2\,^3P_{1,F}$ resonances in $^{14}N^{5+}$, and the corresponding two-resonances in $^{15}N^{5+}$, with co-and counter-propagating beams, at similar beam energies. This enabled the transition wavenumbers to be obtained from eqn. 6 with a precision of .7 ppm. The main source of error was wave-front curvature (or divergence) effects which were difficult to estimate in the non-TEM_{00} mode laser beam. The narrowest Doppler width obtained was 100 MHz.

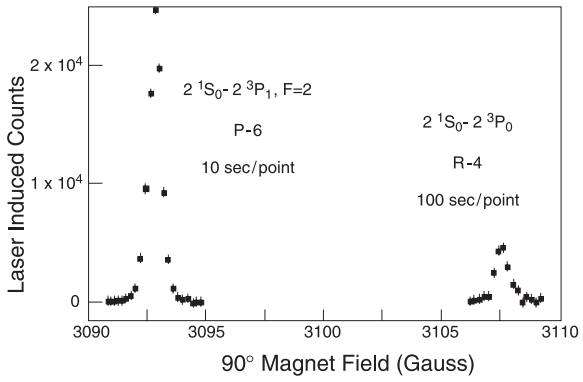

Fig. 9. Doppler-tuned spectrum of the $1s2s\ ^1S_0 - 1s2p\ ^3P_{1,F=2}$ and $1s2s\ ^1S_0 - 1s2p\ ^3P_0$ transitions in $^{14}N^{5+}$

The measured hyperfine splittings of $2\,^3P_1$ level were in reasonable agreement with the relativistic calculations of [96], and also with non-relativistic calculations corrected for relativistic and QED effects [114,115]. The results for the "hyperfine corrected" $2\,^1S_0 - 2\,^3P_1$ interval in $^{14}N^{5+}$ are compared with theory in table 3. QED corrections make up 3.5% of the measured interval. The experiment is hence sensitive to these corrections at the level of 20 ppm, the highest precision for a Lamb shift in any multiply-charged ion.

The closest theoretical result, the "Unified" theory [68], differs by more than 300 times the experimental uncertainty. This discrepancy should be partially removed by analysis including an estimate of the order $(Z\alpha)^4\alpha^2 m_e c^2$ relativistic term and a complete calculation of the two-electron Bethe-logarithm [92]. The $^{14,15}N^{5+}$ $2\,^1S_0 - 2\,^3P_1$ isotope shift was measured to be $-1.6623(10)\,\mathrm{cm}^{-1}$, in fair agreement with an estimate based on [68]. The hyperfine corrected $^3P_0 - ^3P_1$

fine structure intervals for $^{14,15}N^{5+}$ were 8.6707(7) cm^{-1} and 8.6717(10) cm^{-1}, respectively. Because the $0-1$ fine structure splitting in N^{5+} is anomalously small, this measurement is a sensitive test of the theory, see table 4 below.

Table 3. Experimental results for the 1s2s $^1S_0$ – 1s2p $^3P_1$ interval in $^{14}N^{5+}$ compared with theory.

Reference	$\Delta E\,(cm^{-1})$
Myers *et al.* [97]	986.321(7)
Thompson, Howie, and Myers [99]	986.3180(7)
Drake [68]	986.579
Cheng et al. [75,116]	985.9
Plante, Johnson, and Sapirstein [76]	984.7

4.4 $2\,^3P_J - 2\,^3P_{J'}$ Fine Structure Transitions in F^{7+} and Mg^{10+}

The original measurement of the $1s2p\ ^3P_2 - {}^3P_1$ fine structure interval in F^{7+} using a CO_2 laser was also carried out intracavity, but with an ion-laser beam angle of 5° [2,5]. Transitions to the $2\,^3P_1$ level were detected via the 731 eV decay to the ground state, using a proportional counter. The background was mainly from the hyperfine-induced E1 decay of the $2\,^3P_0$ level, and the M2 decay of $2\,^3P_2$, but also from cascade feeding into other, shorter lived, X-ray producing states. The signal to background was always less than 0.1%. The beam velocity was calibrated using nuclear resonances excited in H_2 and CH_4 gas targets. The precision, 20 ppm for the fine structure interval, was limited by uncertainty in the energy of the F^{7+} $2\,^3P$ ions, compared to the mean energy of ions in the foil stripped beam. Nevertheless the result was 100 times more precise than that obtained from UV spectroscopy [103]. It provided very clear confirmation of the order $(Z\alpha)^4\alpha^2 m_e c^2$ term not included in the "Unified theory", but included in the relativistic theories [73,74,75,76], ten years later.

More recently, using a modification of the setup in fig. 8, the co- and counter-propagating laser beam technique was used to measure products of the three $2\,^3P_{2,F} - 2\,^3P_{1,F'}$ fine structure intervals in $^{19}F^{7+}$, in pairs [100]. Since the lifetime of $2\,^3P_2$ is 10.4 ns, it was necessary to place the foil 16 cm upbeam of the interaction region, and use a specially designed, compact, permanent magnet to deflect the ion beam 5° to merge it with the laser beam. The co-linear geometry and improvements to the laser increased the signal-to-background ratio about a factor of 10. The hyperfine splittings were in agreement with [96,115] enabling correction for mixing of the fine structure levels. A precision of nearly 1 ppm was obtained for the centroid of the multiplet. The result was in excellent agreement with, but 16 times more precise than the earlier measurement [2,5].

Using a similar arrangement the $2\,^3P_0 - 2\,^3P_1$ interval in $^{24}Mg^{10+}$ was measured to better than 20 ppm [101], see fig. 10. The maximum laser induced signal was only .3% of the X-ray background. The transition, near 12.0 μm, could only be induced with a co-propagating beam from the long wavelength end of the hot-band of $^{12}C^{16}O_2$. The ion beam velocity was calibrated by tuning $^{14}N^{5+}$ beams at similar rigidity through both the 90° and 5° magnets, and inducing the previously measured $^{14}N^{5+}$ $2\,^1S_0 - 2\,^3P_{1,F}$ resonances.

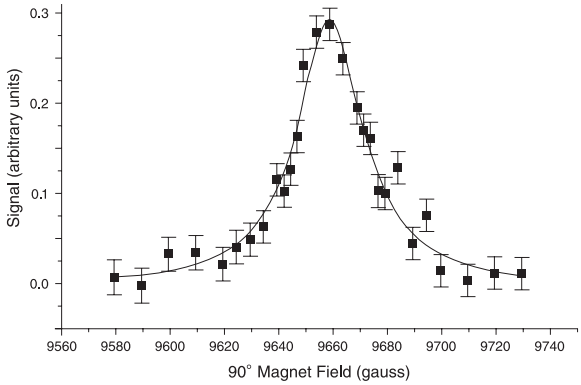

Fig. 10. Doppler-tuned spectrum of the $1s2p\ ^3P_0 - 1s2p\ ^3P_1$ transition in $^{24}Mg^{10+}$

The results for the fine structure measurements in N^{5+}, F^{7+} and Mg^{10+} are summarized in table 4. In fig. 11 they are compared with theory and other precision measurements $Z \leq 12$. The scaling factor $Z(Z-1)^5\alpha^7 m_e c^2$ is the order of the spin-dependent part of the one-electron self-energy [88]. As the figure shows, the sensitivity of the recent measurements to QED corrections of this order, matches or exceeds that of the high precision measurements in helium.

Table 4. Experimental results for the 1s2p $^3P_{J-J'}$ fine structure intervals compared with theory, units cm^{-1}. (The calculations of Zhang *et al.* are incomplete at the level of $\alpha^7 m_e c^2$)

Reference	N^{5+} 0-1	F^{7+} 1-2	Mg^{10+}, 0-1
Experiment [2]		957.883(19)	
Experiment [99,100,101]	8.6707(7)	957.8730(12)	833.133(15)
Zhang, Yan and Drake [89]	8.686	957.840	832.335
Plante, Johnson, and Sapirstein [76]	8.73	957.87	833.1
Chen, Cheng and Johnson [74]	8.67	957.85	833.3

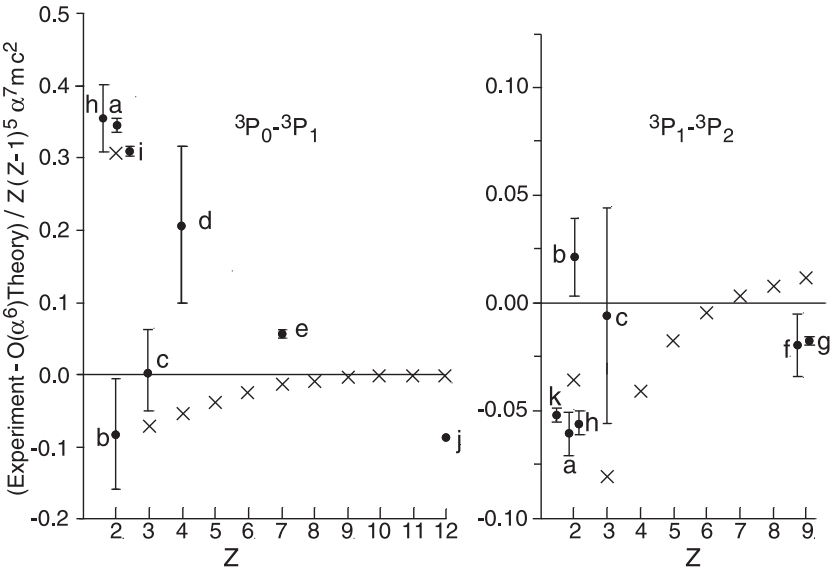

Fig. 11. Results of precision experiments for the $2\,^3\mathrm{P}_0 - 2\,^3\mathrm{P}_1$ and $2\,^3\mathrm{P}_1 - 2\,^3\mathrm{P}_2$ fine structure intervals for $2 \le Z \le 12$, compared with the $O(\alpha^6 m_e c^2)$ theory of Yan and Drake [88] (baseline). The $O(\alpha^7 \ln \alpha)$ corrections of Zhang, Yan and Drake [89] are indicated by crosses. The experimental points are as follows: a) Shiner *et al.* [117], b) Lewis *et al.* [118], and Frieze *et al.* [119], c) Riis *et al.* [106], d) Scholl *et al.* [107], e) Thompson *et al.* [99], f) Myers *et al.* [2], g) Myers *et al.* [100], h) Storry *et al.* [120,121], i) Minardi *et al.* [122], j) Myers *et al.* [101], k) Castillega *et al.* [123]. On this scale, the error bar for magnesium is contained within the point shown

4.5 Future Prospects

Preliminary work on $2\,^3S - 2\,^3P$ measurements in C^{4+} has already taken place [124] and higher-Z ions can be studied as techniques for UV laser spectroscopy develop. The $2\,^1S_0 - 2\,^3P_1$ measurements can be extended to C^{4+} using a far-infrared laser, and to Si^{12+} using a Nd:YAG laser. Direct $2\,^3P_J - 2\,^3P_{J'}$ fine structure measurements can also be extended to higher and lower Z, using appropriate lasers. The precision of these measurements can also be increased should developments in theory justify it.

5 Conclusions

Obtaining experimental tests of the theory of hydrogen-like ions at moderate Z is challenging. Except for hydrogen there appear to be no measurements more precise than current theory. In the next decade, small but significant improvements in precision can be expected for $Z = 2$, 7 and 14. For moderate-Z helium-like ions, laser techniques probe relativistic QED effects at higher precision than

current theory. Measurements can be extended to higher Z and increased in precision. It is hoped this will stimulate further theoretical effort.

Acknowledgments

The author's work at Florida State University has been assisted by many people, most notably J.K. Thompson, H.S. Margolis and M.R. Tarbutt.

References

1. H.W. Kugel and D.E. Murnick: Rep. Prog. Phys. **40**, 297 (1977)
2. E.G. Myers: Nucl. Instr. Meth. B**9**, 662 (1985)
3. F.M. Pipkin in: *Quantum Electrodynamics*, ed. T. Kinoshita, (World Scientific, Singapore 1990), pp. 696–773
4. H.W. Kugel, M. Leventhal, D.E. Murnick, C.K.N. Patel, and O.R. Wood: Phys. Rev. Lett. **35**, 647 (1975)
5. E.G. Myers, P. Kuske, H.J. Andrä, I.A. Armour, N.A. Jelley, H.A. Klein, J.D. Silver, and E. Träbert: Phys. Rev. Lett. **47**, 87 (1981)
6. K. Shima, N. Kuno, M. Yamanouchi, and H. Tawara: At. Data Nucl. Data Tables **51**, 173 (1992)
7. M.A. Levine, R.E. Marrs, J.R. Henderson, D.A. Knapp, and M.B. Schneider: Physica Scripta, T**22**, 157 (1988)
8. P. Kusch and V. W. Hughes in: *Handbuch der Physik XXXVII/1*, ed. by S. Flügge (Springer, Berlin, Heidelberg 1959) pp. 1–172
9. J.D. Jackson: *Classical Electrodynamics*, 3rd edn. (Wiley, New York 1999)
10. I. I. Sobelman: *Atomic Spectra and Radiative Transitions*, 2nd edn. (Springer, Berlin, Heidelberg 1996)
11. B. Franzke: Nucl. Instr. Meth. B**24/25**, 18 (1987)
12. M. Steck *et al.*: Phys. Rev. Lett. **77**, 3803 (1996)
13. S. Schröder *et al.*: Phys. Rev. Lett. **64**, 2901 (1990)
14. J.S. Hangst, M. Kristensen, J.S. Nielsen, O. Poulsen, J.P. Schiffer, and P. Shi: Phys. Rev. Lett. **67**, 1238 (1991)
15. R. Grieser *et al.*: Nucl. Phys. A**626**, 499c (1997)
16. E. Huenges, H. Vonach and J. Labetzki: Nucl. Instrum. Methods **121**, 307 (1974)
17. A. Yariv: *Quantum Electronics*, 3rd edn. (Wiley, New York 1989)
18. R. Dörner, V. Mergel, O. Jagutzki, L. Spielberger, J. Ullrich, R. Moshammer, H. Schmidt-Böcking: Phys. Reports **330**, 95 (2000)
19. M.A. Abdallah, C.R. Vane, C.C. Havener, D.R. Schulz, H.F. Krause, N. Jones, and S. Datz: Phys. Rev. Lett. **85**, 278 (2000)
20. G. Melin: Int. J. Mass Spectr. **192**, 87 (1999)
21. E.D. Donets, in: *The Physics and Technology of Ion Sources*, ed. I.G. Brown (Wiley, New York 1989) p. 245
22. R.E. Marrs: Nucl. Instr. Meth. B**149**, 182 (1999)
23. D.S. Fisher, C.W. Fehrenbach, S.R. Lundeen, E.A. Hessels, B.D. DePaola: Phys. Rev. Lett. **81**, 1817 (1998)
24. S. Borneis *et al.*: Phys. Rev. Lett. **72**, 207 (1994)
25. T. Schüssler, U. Schramm, M. Grieser, D. Habs, T. Rüter, D. Schwalm, A. Wolf: Nucl. Instr. Meth. B**98**, 146 (1995)

26. G. Saathoff, *et al.*: Hyperfine Interact. (in press)
27. J.R. Crespo López-Urritia, B. Bapat, and J. Ullrich: presented at the conference *Hydrogen Atom 2* (unpublished)
28. D. Schneider, D.A. Church, G. Weinberg, J. Steiger, B. Beck, J. McDonald, E. Magee, and D. Knapp: Rev. Sci. Instrum. **65**, 3472 (1994)
29. N. Hermanspahn, H. Häffner, H.-J. Kluge, W. Quint, S. Stahl, J. Verdú, and G. Werth: Phys. Rev. Lett. **84**, 427 (2000)
30. H.A. Klein, H.S. Margolis, J.L. Flowers, K. Gaarde-Widdowson, K. Hosaka, J.D. Silver, M.R. Tarbutt, S.Ohtani, and D.J.E. Knight: *this edition* pp. 664–671
31. W.R. Johnson and G. Soff: At. Data. Nucl. Data Tables **33**, 405 (1985)
32. J.R. Sapirstein and D.R. Yennie: in: *Quantum Electrodynamics*, ed. T. Kinoshita, (World Scientific, Singapore 1990) pp. 560–672
33. K.Pachucki: Hyperfine Interact. **114**, 55 (1998)
34. M. I. Eides, H. Grotch, V.A. Shelyuto: Physics Reports (in press)
35. P.J. Mohr, G. Plunien, and G. Soff: Physics Reports **293**, 227 (1998)
36. W.E. Lamb and R.C. Retherford: Phys. Rev. **72**, 241 (1947)
37. P.J. Mohr: in: *Atomic, Molecular and Optical Physics Handbook*, ed. G.W.F. Drake, (AIP, Woodbury, NY 1996) pp. 341–351
38. U.D. Jentschura, P.J. Mohr, and G. Soff: Phys. Rev. Lett. **82**, 53 (1999)
39. H.F. Beyer: IEEE Trans. Instrum. Meas. **44**, 510 (1995)
40. T. Stöhlker *et al.*: Phys. Rev. Lett. (in press)
41. K. Pachucki: Phys. Rev. Lett. **72**, 3154 (1994)
42. M.I. Eides and V.A. Shelyuto: JETP Lett.**61**, 478 (1995)
43. S. Mallampalli and J. Sapirstein: Phys. Rev. Lett. **80**, 5297 (1998)
44. I. Goidenko, L. Labzowsky, A. Nefiodov, G. Plunien, and G. Soff: Phys. Rev. Lett. **83**, 2312 (1999)
45. V.A. Yerokhin: Phys. Rev. A**62**, 12508 (2000)
46. S.G. Karshenboim: JETP **76**, 541 (1993)
47. C. Schwob *et al.*: Phys. Rev. Lett. **82**, 4960 (1999)
48. D.J. Berkeland, E.A. Hinds, and M. G. Boshier: Phys. Rev. Lett. **75**, 2470 (1995)
49. M. Niering *et al.*: Phys. Rev. Lett. **84**, 5496 (2000)
50. H.A. Bethe and E.E. Salpeter in: *Handbuch der Physik XXXV*. ed. by S. Flügge (Springer, Berlin, Heidelberg 1957) pp. 88–436
51. S.P. Goldman and G.W.F. Drake: Phys. Rev. **24**, 183 (1981)
52. F.A. Parpia and W.R. Johnson: Phys. Rev. A**26**, 1142 (1982)
53. M.R. Tarbutt, D. Crosby, E.G. Myers, N. Nakamura, S. Ohtani, and J.D. Silver: *this edition*, pp. 727–736
54. G. Hölzer *et al.*: Phys. Rev. A**57**, 945 (1998)
55. O.R. Wood, C.K.N. Patel, D.E. Murnick, E.T. Nelson, M. Leventhal, H.W. Kugel, and Y. Niv: Phys. Rev. Lett. **48**, 398 (1982)
56. P. Pellegrin, Y. El Masri, L. Palffy, and R. Prieels: Phys. Rev. Lett. **49**, 1762 (1982)
57. A.P. Georgiadis, D. Müller, H.-D. Sträter, J. Gassen, P. von Brentano, J.C. Sens, and A. Pape: Phys. Lett. A **115**, 108, (1986)
58. H.-J. Pross, D. Budelsky, L. Kremer, D. Platte, P. von Brentano, J. Gassen, D. Muller, F. Scheuer, A. Pape, and J.C. Sens: Phys. Rev. A **48**, 1875 (1993)
59. V. Zacek, H. Bohn, H. Brum, T. Faestermann, F. von Feilitzsch, G. Giorginis, P. Kienle, and S. Schuhbeck: Z. Phys. A **318**, 7 (1984)
60. H. Gould and R. Marrus: Phys. Rev. A**28**, 2001 (1983)

61. E.G. Myers and M.R. Tarbutt: *this edition*, pp. 688–698; E.G. Myers, M.R. Tarbutt, V.G. Ivanov, and S.G. Karshenboim, to be published
62. E.G. Myers, R. Hankins, J.D. Silver and M.R. Tarbutt: Hyperfine Interact. (in press)
63. S.A. Burrows, S. Guérandel, E.A. Hinds, F. Lison, and M.G. Boshier: *this edition*, pp. 303–313
64. A. van Wijngaarden, F. Holuj, and G.W.F. Drake: Phys. Rev. A, in press
65. I. Klaft *et al.*: Phys. Rev. Lett. **73**, 2425 (1994)
66. P. Seelig *et al.*: Phys. Rev. Lett. **81**, 4824 (1998)
67. Y. Accad, C.L. Pekeris, and B. Schiff: Phys. Rev. A**4**, 516 (1971)
68. G.W.F. Drake: Can. J. Phys. **66**, 586 (1988)
69. H. Araki: Prog. Theor. Phys. **17**, 619 (1957)
70. P.K. Kabir and E.E. Salpeter: Phys. Rev. **108**, 1256 (1957)
71. J. Sucher: Phys. Rev. **109**, 1010 (1958)
72. J. Sucher: Phys. Rev. A**22**, 348 (1980)
73. W.R. Johnson and J. Sapirstein: Phys. Rev. A**46**, 2197 (1992)
74. M.H. Chen, K.T. Cheng, and W.R. Johnson: Phys. Rev. A**47**, 3692 (1993)
75. K.T. Cheng, M.H. Chen, W.R. Johnson, and J. Sapirstein: Phys. Rev. A**50**, 247 (1994)
76. D.R. Plante, W.R. Johnson, and J. Sapirstein: Phys. Rev. A**49**, 3519 (1994)
77. P. Indelicato: Phys. Rev. A**51**, 1132 (1995)
78. I. Lindgren: Int. J. Quantum Chemist. **57**, 683 (1996)
79. P.J. Mohr: Nucl. Instr. Meth. B**87**, 232 (1994)
80. H. Persson, S. Salomonson, P. Sunnergren, and I. Lindgren: Phys. Rev. Lett. **76**, 204 (1996)
81. B. Asén, S. Salomonson, and I. Lindgren: presented at the conference *Hydrogen Atom 2* (unpublished)
82. O. Andreev and L. Labzowsky: *this edition*, pp. 591–604
83. G.W.F. Drake and W.C. Martin: Can. J. Phys. **76**, 679 (1998)
84. G.W.F. Drake, in: *Long Range Casimir Forces: Theory and Recent Experiment on Atomic Systems*, ed. F.S. Levin and D.A. Micha, (Plenum, New York, 1993) pp. 107–218
85. K. Pachucki: J. Phys. B**31**, 2489 (1998); **31** 3547 (1998)
86. T. Zhang: Phys. Rev. A**53**, 3896 (1996); Phys. Rev. A**54**, 1252 (1996); T. Zhang and G.W.F. Drake: Phys. Rev. Lett. **72**, 4078 (1994)
87. K. Pachucki: J. Phys. B**32**, 137 (1999)
88. Z.-C. Yan and G.W.F. Drake: Phys. Rev. Lett. **74**, 4791 (1995)
89. T. Zhang, Z.-C. Yan, and G.W.F. Drake: Phys. Rev. Lett. **77**, 1715 (1996)
90. G.W.F. Drake: private communication
91. K. Pachucki and J. Sapirstein: presented at the conference *Hydrogen Atom 2*, and to be published
92. G.W.F. Drake and S.P. Goldman: Can. J. Phys. **77**, 835 (1999)
93. R. Marrus and R.W. Schmieder: Phys. Rev. A**5**, 1160 (1972)
94. W.R. Johnson, D.R. Plante and J. Sapirstein: Adv. At. Mol. Opt. Phys. **35**, 255 (1995)
95. A. Derevianko and W.R. Johnson: Phys. Rev. A**56**, 1288 (1997)
96. W.R. Johnson, K.T. Cheng, and D.R. Plante: Phys. Rev. A**55**, 2728 (1997)
97. E.G. Myers, J.K. Thompson, E.P. Gavathas, N.R. Claussen, J.D. Silver, and D.J.H. Howie: Phys. Rev. Lett. **75**, 3637 (1995)
98. E.G. Myers, D.J.H. Howie, J.K. Thompson, and J.D. Silver: Phys. Rev. Lett. **76**, 4899 (1996)

99. J.K. Thompson, D.J.H. Howie, and E.G. Myers: Phys. Rev. A**57**, 180 (1998)
100. E.G. Myers, H.S. Margolis, J.K. Thompson, M.A. Farmer, J.D. Silver, and M.R. Tarbutt: Phys. Rev. Lett. **82**, 4200 (1999)
101. E.G. Myers and M.R. Tarbutt: Phys. Rev.A **61**, 10501(R) (1999)
102. D.J.H. Howie, J.D. Silver, and E.G. Myers: J.Phys. B**29**, 927 (1996)
103. H.A. Klein, F. Moscatelli, E.G. Myers, E.H. Pinnington, J.D. Silver, and E. Traebert: J. Phys. B. **18**, 1483 (1985)
104. K.W. Kukla *et al.*: Phys. Rev. A**51**, 1905 (1995)
105. W. Curdt, E. Landi, K. Wilhelm, and U. Feldman: Phys. Rev. A**62**, 22502 (2000)
106. E. Riis, A.G. Sinclair, O. Poulsen, G.W.F. Drake, W.R.C. Rowley, and A.P. Levick: Phys. Rev. A **49**, 207 (1994)
107. T.J. Scholl, R. Cameron, S.D. Rosner, L. Zhang, R.A. Holt, C.J. Sansonetti, and J.D. Gillaspy: Phys. Rev. Lett. **71**, 2188 (1993)
108. T.P. Dinneen, N. Berrah-Mansour, H.G. Berry, L. Young, and R.C. Pardo: Phys. Rev. Lett. **66**, 2859 (1991)
109. R.A. Holt, S.D. Rosner, T.D. Gaily, and A.G. Adam: Phys. Rev. A**22**, 1563 (1980)
110. M. Englert *et al.*: Appl. Phys. B**28**, 81 (1982)
111. E. Riis, H.G. Berry, O. Poulsen, S.A. Lee, and S.Y. Tang: Phys. Rev. A**33**, 3023 (1986)
112. T.J. Scholl, R.A. Holt, and S.D. Rosner: Phys. Rev. A**39**, 1163 (1989)
113. L.C Bradley, K.L. Soohoo, and C. Freed: IEEE J. Quant. Elect., QE-22, 234 (1986)
114. K. Ohtsuki and K. Hijikata: J. Phys. Soc. Jpn. **57**, 4150 (1988)
115. L. Pan and G.W.F. Drake: (private communication 1998)
116. The result quoted here uses the relativistic energy from [75] with QED corrections from [68]
117. D. Shiner, R. Dixson, and P. Zhao: Phys. Rev. Lett. **72**, 1802 (1994); R. Dixson and D. Shiner: Bull. Am. Phys. Soc. **39**, 1059 (1994)
118. S.A. Lewis, F.M.J. Pichanick, and V.W. Hughes: Phys. Rev. A **2**, 86 (1970)
119. W. Frieze, E.A. Hinds, V.W. Hughes, and F.M.J. Pichanick: Phys. Rev. A **24**, 279 (1981)
120. C.H. Storry and E.A. Hessels: Phys. Rev. A**58**, R8 (1998)
121. C.H. Storry, M.C. George, and E.A. Hessels: Phys. Rev. Lett. **84**, 3274 (2000)
122. F. Minardi, G. Bianchini, P. Cancio Pastor, G. Giusfredi, F.S. Pavone, and M. Inguscio: Phys. Rev. Lett. **82**, 1112 (1999)
123. J. Castillega, D. Livingston, A. Sanders, and D. Shiner: Phys. Rev. Lett. **84**, 4321 (2000)
124. L. Young: (private communication); E. Pinnington: (private communication)